Chapter 2

Physics Overview

As a consequence of the presently accepted theory of strong interactions it is expected that a deconfined state of quark and gluon matter, the quark–gluon plasma, exists. Such a plasma should occur over a broad range in density and temperature. The underlying mechanism that brings about this deconfined state is the screening of the color field, not unlike the Debye screening of the electric field in a solid. QCD lattice calculations confirm the existence of a well defined phase transition signaling the onset of this state.

It is generally conjectured that the quark–gluon plasma may be created in high energy nucleus–nucleus collisions under a broad range of conditions which are bounded in one direction by high baryon density and low temperature, and in the other by zero net baryon density and temperatures above the Hagedorn limit. The first situation, according to current wisdom, is appropriate to the stopping regime of up to $\sqrt{s} \approx 10$ GeV per pair of nucleons, where stopping of the projectile results in high baryon and energy density. This regime is now being studied in the heavy ion fixed target experiments at the AGS and the CERN–SPS.

The creation of the baryon–poor, high–temperature plasma, on the other hand, depends on attaining collision energies far above the stopping regime. The colliding nuclei will then pass through one another and the baryon-rich regions will be close to the original nuclei in rapidity. After the collision has occurred, a strong color field is created in the space between the nuclei which is anticipated to create a quark–gluon plasma with about an equal number of baryons and anti-baryons. It may be pointed out that while the phase transition to the quark–gluon plasma with zero net baryon density has been modeled in lattice QCD calculations, this has not as yet been possible for the baryon-rich situation. The phase transition to the plasma is expected to be more likely for central collisions, with most of the colliding nucleons participating in the process, while peripheral collisions should behave more like elementary nucleon–nucleon interactions.

At RHIC opportunities exists for experiments investigating both the relatively baryon–poor quark-gluon plasma in the midrapidity region and the baryon-rich plasma in the fragmentation regions of rapidity.

2.1 Motivation

The most basic information available for understanding the phenomena that occur in heavy ion collisions comes from the momentum spectra and yields of the various emitted particles as a function of transverse momentum, p_t, and rapidity, y. It is one goal of this experiment to measure these spectra in the kinematic regions in which they are most sensitive to model predictions. Particle yields, as a function of y, are important indicators of the densities obtained in the collisions and of the produced entropy. The spectral shapes and slopes and their y-dependence reveal the reaction dynamics and the degree of thermalization attained. The high p_t parts of the spectra are indicators of the early phases of the reaction. Enhancement of strangeness and/or antibaryons may signal the creation of the quark–gluon plasma.

As an example of the importance of these measurements, the expectations for the "baryon free" region for Au+Au central collisions at RHIC are compared for three different calculations, all of which are based in part on theoretical string models and in part on scaling from p+p data, particularly from the CERN ISR ($\sqrt{s} = 64$ GeV.) Plotted in Fig. 2.1 is the rapidity density for the net baryon number, namely the multiplicity of $\mathrm{p} - \bar{\mathrm{p}} + \mathrm{n} - \bar{\mathrm{n}}$ (after all unstable particles have decayed).

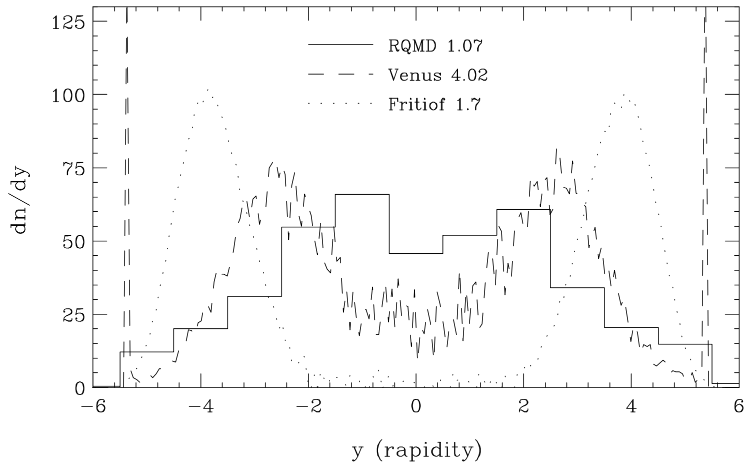

Figure 2.1: Net baryons from central Au+Au collisions

The FRITIOF 1.7 model[1], which describes the p+p data of the ISR quite well, predicts a flat, baryon-poor region in midrapidity for central Au+Au collisions at RHIC, and peaks at $y = \pm 3.8$, shifted 1.6 units from the beam rapidity of ± 5.4. The prediction of the VENUS 4.02 code[2] for the same system is dramatically different from FRITIOF, showing no baryon free region, and smaller peaks at $y = \pm 2.6$. Thus the increased "stopping" inherent in VENUS has spread the colliding baryons over the whole rapidity region. RQMD[3] is a transport model which also incorporates a string breaking scheme. It predicts[4] even more piling up of net baryon number at midrapidity than does VENUS. Thus this important indicator of baryon density is very much model-dependent, emphasizing the need for measurements in as broad a rapidity range as possible.

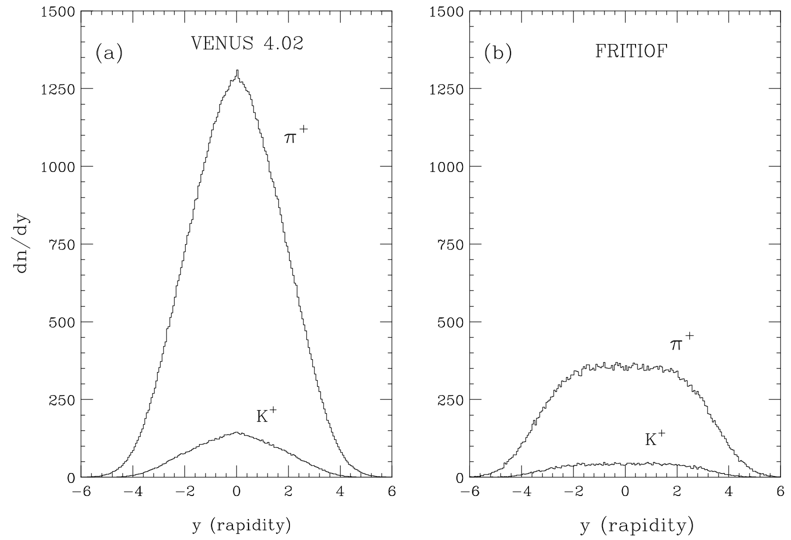

Figure 2.2: Distributions of dn/dy for positive pions and kaons in central Au+Au collisions

Figure 2.2 shows a comparison of the rapidity distributions for π^+ and K^+ mesons, from VENUS (Fig. 2.2a), and from FRITIOF (Fig. 2.2b). Again FRITIOF yields a flat, boost-invariant, midrapidity region, while VENUS predicts distributions that are nowhere flat. Also the overall π^+ multiplicity is larger in VENUS by a factor of 2. In the VENUS model the baryon and energy densities change with rapidity over the entire range, and hence the physics of the collision system also depends on rapidity.

This discussion has shown the importance of measuring the actual rapidity dependence of the baryon and meson yields, but equally strong arguments can be made for also measuring the baryon and meson p_t distributions over as wide a range of rapidity as possible. Furthermore, it is important to systematically study these distributions as a function of the mass of the projectiles as well as the violence (impact parameter) of the collision. Such information is critically needed to establish constraints on the theoretical models and for understanding the basic physical processes for heavy ion collisions at

RHIC.

Global measurements of charged particles give information on the multiplicity density, and thus the energy density achieved in the reactions. It is anticipated that a sufficiently large density, which is a necessary condition for the formation of QGP, can be reached in central Au+Au collisions at RHIC. Thus the multiplicity information is an integral part of the measurements of the hadronic spectra in the BRAHMS Experiment. As an example of this, the dependence of $< p_t >$ on $dN/d\eta$ may signal a phase transition (Ref. 6).

2.2 Physics Goals and Experimental Criteria

In the present section the physics motivation is translated into performance criteria for the Forward and Midrapidity Spectrometers of BRAHMS. The required rapidity and p_t coverages come in part from model calculations and in part from extrapolations of p+p data, particularly from the ISR. The spectrometers are designed so as to handle the predictions from the models in terms of both kinematical coverage and particle densities in the detectors, and have a considerable safety margin.

The criterion adopted for the selection of a forward rapidity limit for created particles is that the measurements should extend over a sufficiently large range that the predicted distributions change by at least a factor of two from their midrapidity values. For protons the maximum rapidity is chosen to be $y = 3.5$. Although it is desirable to come closer to $y = 4$, the technical difficulties are formidable because of the extreme forward angles needed ($\theta \approx 1°$). The more realistic limit of $y = 3.5$ is a compromise which will certainly allow us to establish the trend of the net proton multiplicity $< p > - < \bar{p} >$ at large rapidities.

As mentioned above (see Figs. 2.1 and 2.2) the models predict rapidity distributions which vary from a flat midrapidity plateau to distributions which change over the whole rapidity range. It is thus critically important to measure the complete rapidity distribution (down to $y = 0$) under the same trigger conditions.

At each rapidity the accepted p_t range should be at least large enough to determine the integral over the $dN/d(p_t^2)$ distribution to good accuracy (5%) and to determine the shape of the spectrum (i.e., its slope). In addition, it is desirable to have enough range (and counting statistics) to observe deviations from the shape expected from p+p collisions; this is exponential at low p_t and a power law at larger values (Ref. 7). Model predictions are used to judge the p_t coverage needed. Figure 2.3 shows some momentum spectra at selected angles, 3°, 5°, 15°, 25°, 45°, and 90°, for Au+Au$\rightarrow \pi^+ + X$ and p+X, all from VENUS.

The cross section integrals are determined sufficiently by measurements to ≈ 2 times the mean value in p_t, while a good determination of the shape requires a measurement down to $\approx 10^{-2}$ of the maximum of the distribution and thus sets the wider range. At

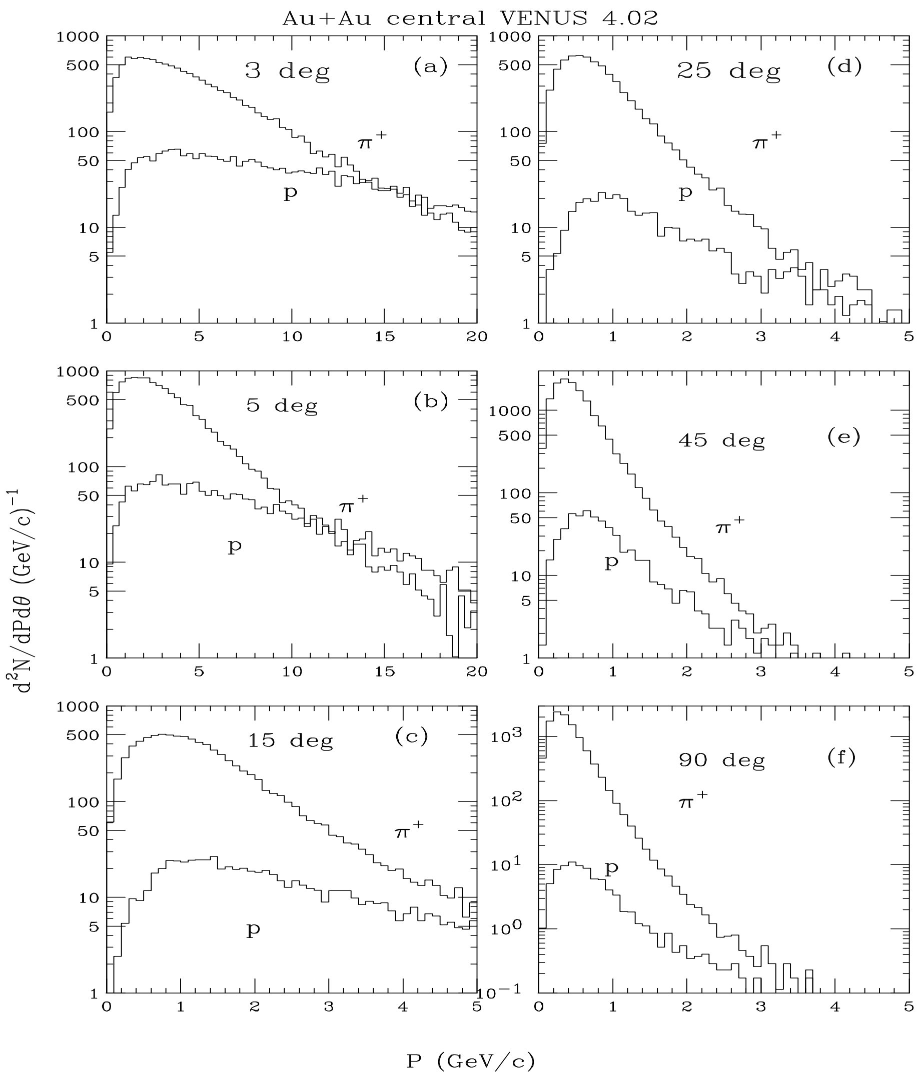

Figure 2.3: $d^2n/dpd\theta$ for several angle settings in central Au+Au collisions

5° the slope criterion gives a required maximum momentum of $\approx$ 17 GeV/c for π^+ and a corresponding value for protons of $\approx$25 GeV/c. Generally, the momentum range thus determined varies roughly as $\approx 1/\sin\theta$ and corresponds to a p_t–range that is independent of angle (and rapidity). The most difficult cases, e.g., a 25 GeV/c particle at 2°, will have $p_t \approx$1.5 GeV/c, corresponding to an invariant cross section that is between 2 and 3 orders of magnitude down from the maximum (using a slope parameter of 250 GeV/c). However, it is emphasized that apart from the very forward angles (2°–3°) the p_t range of the instrument is much larger than 1.5 GeV/c. At 10°, e.g., p_t up to 4.3 GeV/c can be measured. The instrumental limit is in momentum, not in transverse momentum. At

90° the acceptance can be up to a p_t of 5 GeV/c.

It is difficult to establish a criterion for the lower value of measurement in p_t. To avoid missing important spectral components it should be as low as possible. Momenta of $\simeq$2 GeV/c for protons and pions can be measured at forward angles, which leads to the very low p_t cutoff of $\simeq$100 MeV/c. At midrapidity the low momentum limit is determined more by identification problems due to decay losses, multiple scattering and energy losses. It can be $\sim$100 MeV/c for pions.

The measurement of composite baryons and in particular anti-baryons ($\bar{\mathrm{d}}$, $\bar{\mathrm{t}}$, and $^3\bar{\mathrm{He}}$) is possible in BRAHMS. The latter may constitute a very sensitive probe of the production of nonstrange anti-baryons through the mechanism of coalescence.

2.3 Pair Correlations

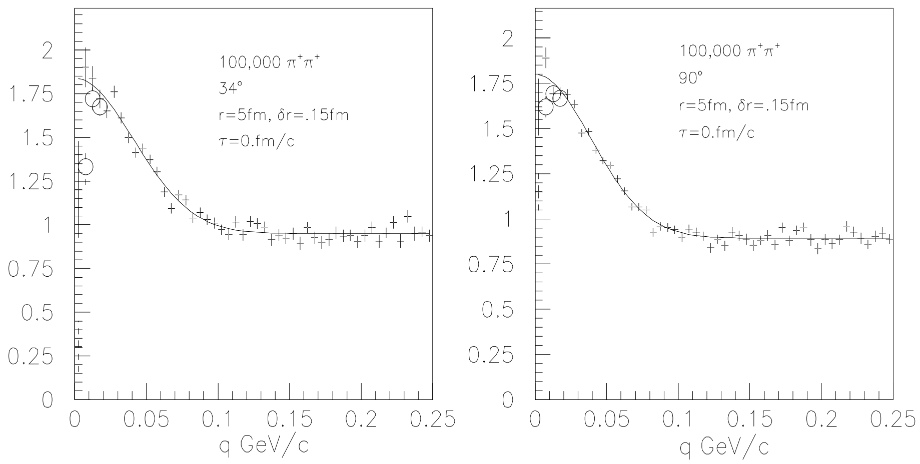

Figure 2.4: The $\pi^+\pi^+$ correlation function for the midrapidity spectrometer at 34 and 90°. The open circles at small q show the distortion caused if all pairs are lost with a spatial separation less than 1 cm in the front TPC.

The correlation of like-bosons as a function of relative momentum can provide a measure of the space-time structure of the emission source. Measurement of spatial source size combined with particle spectra and yields can provide insight into the dynamics which controlled the evolution from an initial hot dense phase to the final hadronized state. To illustrate the capability of the midrapidity spectrometer to measure like-boson correlations, we have simulated a Gaussian source with a radius of 5 fm and a lifetime of 0 fm/c. Figure 2.4 shows the resultant correlation functions obtained from π^+ pairs with the spectrometer at 34° and 90°. It is expected that a correlation function of 100,000 like sign pairs could be obtained in less than eight hours. Figure 2.5 shows the correlation function obtained from 100,000 K^+ pairs with the spectrometer at 34°. Also shown is the two-particle density as a function of q and q_0. Typically a few days of running would be required to obtain 100,000 K^+ pairs. Naturally, the modest aperture of our experiment does not enable the type of systematic measurements that a large solid angle detector can perform, but it should provide complementary results. We are presently investigating the systematics involved in this type of analysis.

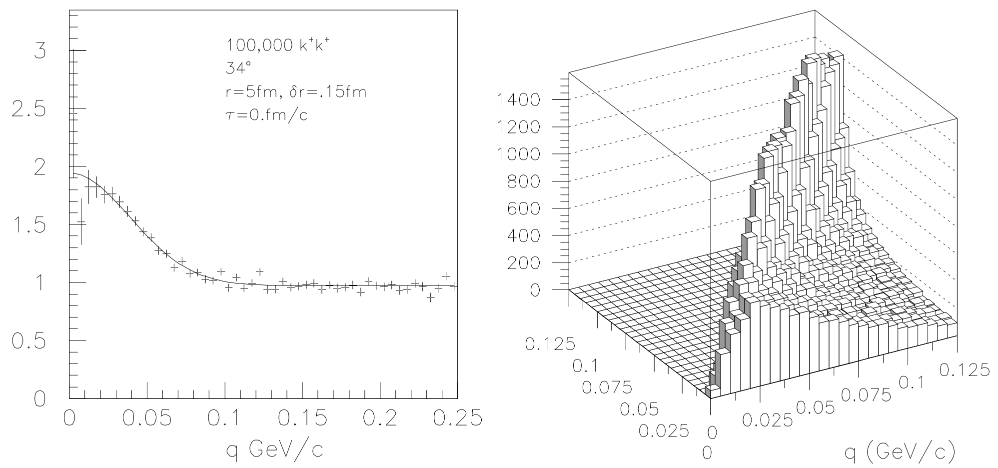

Figure 2.5: The K^+K^+ correlation function obtained with the midrapidity spectrometer at 34°. The pair density as a function of q and q_0 is also shown.

2.4 $\phi(1020)$ Measurement

One of the potential signatures of QGP involves the measurements of ϕ production in ultra-relativistic heavy-ion collisions[8,9,10]. Modifications to the width and mass of the ϕ, e.g. caused by a chiral symmetry restoration, and in particular a study of the p_t dependence of such effects, might constitute a signature of QGP formation, since the low p_t ϕ's will decay inside the hadronic fireball.

The BRAHMS midrapidity spectrometer (see Section 3.2), with its reasonable solid angle and good hadron identification, can be utilized to study ϕ meson production dynamics from Au+Au collisions at RHIC energy via its decay to K^+K^-.

Figure 2.6 shows the distributions of the accepted ϕ mesons in p_t and y (rapidity) space. The calculation is for ϕ detection via the K^+K^- decay mode with the midrapidity spectrometer at 34° and 90° and $\int B \cdot d\ell = 0.28$ T-m. A momentum resolution, $\delta p/p$ = 1.0%, for each component of the momentum is assumed in the calculation, and the

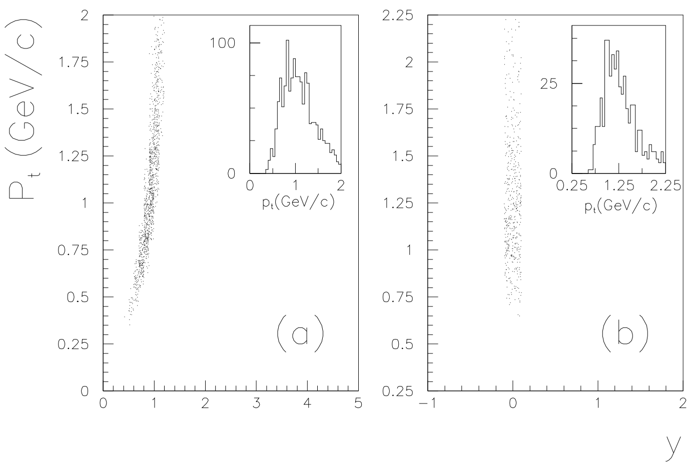

Figure 2.6: Distributions in (y,p_t) space of the accepted ϕ mesons detected through the K^+K^- decay mode, with the midrapidity spectrometer at (a) 34° and (b) 90°. Insets show the accepted p_t distributions.

ϕ mass is distributed according to a Breit-Wigner function with a known width[11]. The expected invariant mass distributions of K^+K^- pairs are shown in Fig. 2.7 for 10 million central Au+Au events with the midrapidity spectrometer at 34° (40 million at 90°) using the prediction of VENUS. 20% of the $K^{\pm}$'s are assumed to come from ϕ's. The solid curve shows the combination of all K^+K^- pairs, and the dashed line in the figure corresponds to the background distribution from the combinations of all the single K^+'s and K^-'s. The insert shows the difference of the solid and dashed curves. This shows that the ϕ can be well reconstructed with $\Gamma \sim 5.7$ MeV from high multiplicity events.

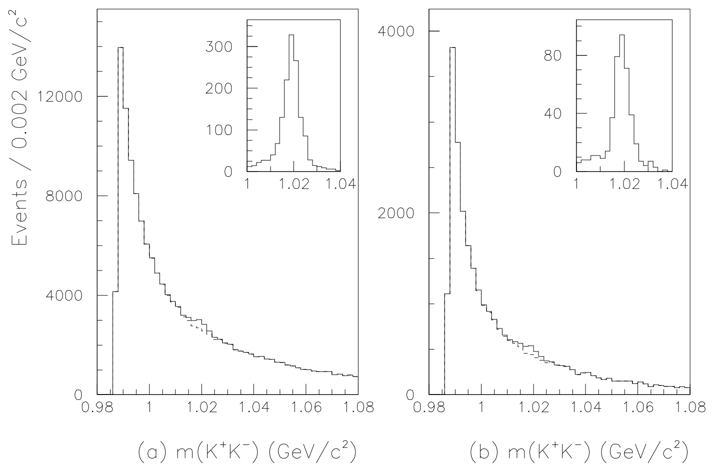

Figure 2.7: The expected invariant mass distributions of K^+K^- pairs with the midrapidity spectrometer at (a) 34° and (b) 90°. The solid curve shows the combination of all K^+K^- pairs, whereas the dashed curve shows the combinatoric background distribution. The inset shows the difference of the solid and dashed curves.

2.5 References

1. B. Andersson, G. Gustafson and B. Nielsson-Almqvist, Nucl. Phys. **B281**, 289 (1987).
2. K. Werner, Z. Physics **C42**, 85 (1989).
3. H. Sorge, H. Stöcker and W. Greiner, Ann. Phys. (N.Y.) **192**, 266 (1989).
4. Th. Schönfeld, *et al.*, Nucl. Phys. **A544**, 439c (1992).
5. D. Beavis, *et al.*, RHIC Letter of Intent #8, Brookhaven National Laboratory, 1990; Addendum, 1991; Revised, 1992.
6. L.Van Hove, Physics Lett **B118**, 138 (1982).
7. C. Albajar *et al.*, Nucl. Phys. **B335**, 261 (1990).
8. A. Shor, Phys. Rev. Lett. **18**, 1122 (1985).
9. P. Koch, U. Heinz and J. Pisút, Phys. Lett. **B243**, 149 (1990).
10. D. Lissauer and E. Shuryak, Phys. Lett. **B253**, 15 (1991).
11. Particle Data Group, Phys. Rev. **D50**, 1173 (1994).